Chemical Science

ROYAL SOCIETY OF CHEMISTRY

EDGE ARTICLE

View Article Online
View Journal | View Issue





Cite this: *Chem. Sci.*, 2022, **13**, 68

All publication charges for this article have been paid for by the Royal Society of Chemistry

Received 14th October 2021
Accepted 29th November 2021

DOI: 10.1039/d1sc05663h

rsc.li/chemical-science

# Linking metal–organic cages pairwise as a design approach for assembling multivariate crystalline materials†

Adrian W. Markwell-Heys, [a] Michael Roemelt, [b] Ashley D. Slattery, [c] Oliver M. Linder-Patton [a] and Witold M. Bloch *[a]

Using metal–organic cages (MOCs) as preformed supermolecular building-blocks (SBBs) is a powerful strategy to design functional metal–organic frameworks (MOFs) with control over the pore architecture and connectivity. However, introducing chemical complexity into the network *via* this route is limited as most methodologies focus on only one type of MOC as the building-block. Herein we present the pairwise linking of MOCs as a design approach to introduce defined chemical complexity into porous materials. Our methodology exploits preferential Rh-aniline coordination and stoichiometric control to rationally link $Cu_4L_4$ and $Rh_4L_4$ MOCs into chemically complex, yet extremely well-defined crystalline solids. This strategy is expected to open up significant new possibilities to design bespoke multi-functional materials with atomistic control over the location and ordering of chemical functionalities.

## Introduction

The ability to rationally integrate multiple chemical entities within a crystalline porous solid is one of the defining goals in the field of metal–organic frameworks (MOFs).[1–3] Such control offers exciting opportunities to design multi-functional materials capable of performing complex and sophisticated operations relevant to applications in gas separation and catalysis.[4–8] However, integrating multiple different metal ions and ligands within a MOF structure is difficult to achieve with the typical 'one-pot' synthesis.[9–11] This relates to the challenge in predicting the assembly outcome of multi-component mixtures and their tendency to crystallise as simple binary phases.[1,12,13]

In contrast, Nature integrates chemical complexity into multi-functional architectures by ordering preorganised subunits in a step-wise manner.[14,15] This elegant, step-wise approach has indeed inspired the design of synthetic porous solids. For example, preformed molecular cages have been co-crystallised into multi-functional solids *via* hydrogen bonding,[16] chiral-recognition,[17] and ionic interactions.[18] However, predicting the crystal structure for solids formed by non-covalent interactions is a long-standing challenge in solid-state chemistry.[19,20]

In light of this, we propose that linking of metal–organic cages (MOCs) by coordination is a rational approach to introduce multiple functionalities into porous solids. In this regard, MOCs with $[M_2(COO)_4(solvent)_2]$ (M = Cu(II), Rh(II) and Cr(II)) paddlewheel sites represent versatile supermolecular building-blocks (SBBs) owing to their exterior coordination sites and compatible ligand-based functionalities.[21,22]

The synthesis of MOFs from MOCs was first demonstrated by Zhou who showed that preformed $Cu_{12}L_{12}$ octahedra could be linked with 4,4′-bipyridine to generate crystals of an interpenetrated MOF (Fig. 1a).[23] More recently, Maspoch and co-workers showed that $Rh_{24}L_{24}$ MOCs can be utilised as SBBs to generate highly-connected MOFs *via* coordination of metal clusters to the cage exterior (Fig. 1b).[24] These methodologies however, are limited to only one type of MOC as the building-block.[25,26] The coordinative linking of two different MOCs represents a significant advancement in the design of multi-functional porous solids, but is hitherto unrealized. This may be due to the increased complexity of such a system, in terms of the challenge of directing the selective coordination of one MOC to another.

Herein we report the pairwise linking of two different MOCs as a design approach for generating an unprecedented class of multivariate crystalline materials (Fig. 1c). The MOC building-blocks utilised in this study are based on a $M_4L_4$ lantern architecture (M = Cu(II) or Rh(II)) and their pairwise linking is achieved by preferential Rh-aniline coordination. The hallmark of this approach is the ability to pre-program the positioning of

[a]*Department of Chemistry, The University of Adelaide, Adelaide, Australia. E-mail: witold.bloch@adelaide.edu.au; Tel: +61 8 8313 5039*

[b]*Institut für Chemie, Humboldt-Universität zu Berlin, Brook-Taylor Str. 2, 12489 Berlin, Germany*

[c]*Adelaide Microscopy, The University of Adelaide, Adelaide 5005, Australia*

† Electronic supplementary information (ESI) available: Full experimental details and supporting analysis. CCDC 2106776–2106778. For ESI and crystallographic data in CIF or other electronic format see DOI: 10.1039/d1sc05663h

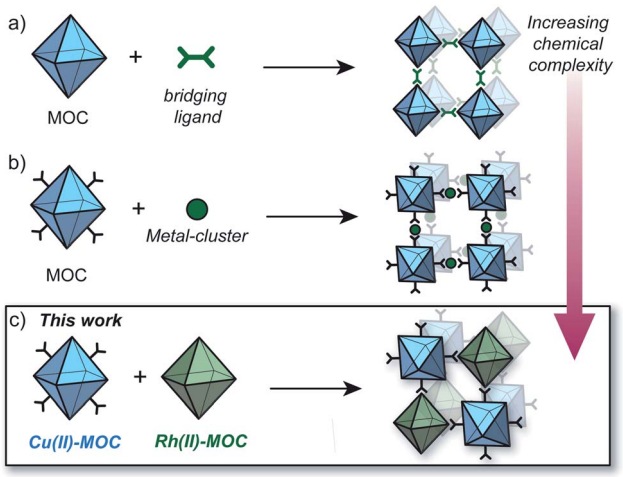


Fig. 1 Strategies to synthesise MOFs from preformed MOCs; (a) utilising bridging ligands to link MOCs *via* the available coordination sites;[23] (b) linking surface-functionalised MOCs *via* a metal cluster;[24] (c) *this work*: linking a surface-functionalised Cu(II) MOC to a Rh(II) MOC *via* preferential Rh-aniline coordination.

multiple metal ions and ligand-based functionalities within a structurally well-defined porous material.

## Results and discussion

### Synthesis of MOC building-blocks

As part of our efforts to design MOCs as SBBs, we recently reported $[Cu_4L_4^1]$ – denoted here as **1-Cu**.[27] **1-Cu** is a soluble cage structure composed of two $[Cu_2(COO)_4(solvent)_2]$ paddlewheel nodes and four ligands based on a fluoroaniline backbone (Fig. 2a). **1-Cu** is a rare example of a MOC that possesses exterior amine groups and vacant coordination sites yet remains stable in solution.‡[28–30]

In order to target a heterogeneous bimetallic system, we prepared a kinetically inert $[Rh_4L_4^2]$ cage as the linking partner. We selected the aldehyde-functionalised ligand $L^2$ based on the established chemistry of the $[Cu_4L_4^2]$ MOC analogue, as well as the ability to explore covalent linking options.[31] Thus, $[Rh_4L_4^2]$ (**2-Rh**, Fig. 2a) was prepared by combining $L^2$, $Rh_2(OAc)_4$ and $Na_2CO_3$ in DMA and heating the resultant mixture at 85 °C for 32 h. Single-crystals of **2-Rh** were grown by slow-vapor diffusion of MeCN into a DMF solution of the cage. Single-crystal X-ray diffraction (SCXRD) confirmed the $M_4L_4$ structure and revealed that the axial paddlewheel sites of the MOC are occupied by MeCN ligands (Fig. S26†).

### Synthesis and structure of mixed-cage MOF 3

In conceptualizing **1-Cu** and **2-Rh** as SBBs, both MOCs represent planar four-connecting nodes when considering the positioning and orientation of their covalent functionalities. However, when combining the two MOCs in DMF, we observed a crystallisation phenomenon that was dominant over their covalent reactivity. A microcrystalline precipitate with a Cu : Rh ratio of 1 : 2 (as determined by EDX analysis) was isolated from a DMF mixture of **1-Cu** and **2-Rh** after 2 h at room temperature. This co-crystallisation, however, did not occur in DMA as the solvent, which enabled us to grow larger crystals of the material for SCXRD analysis.

Slow-vapor diffusion of ethyl acetate into the 1 : 2 mixture of **1-Cu** and **2-Rh** in DMA resulted in the formation of ~200 μm-sized plate-like crystals of $\{[\mathbf{1\text{-}Cu}]\cdot[\mathbf{2\text{-}Rh}]_2\}_n$, (herein denoted as **3**) after 5 days. Synchrotron SCXRD revealed that **3** crystallizes in the tetragonal space group *I*4/*m*. The asymmetric unit contains 1/8 of the structure **1-Cu** and 1/4 of the structure of **2-Rh** (Fig. 2b), which is in agreement with the 1 : 2 Cu : Rh stoichiometry observed by EDX. The X-ray structure reveals that **1-Cu** and **2-Rh** crystallise through coordinative linking; the exterior coordination sites of **2-Rh** are both occupied by an aniline

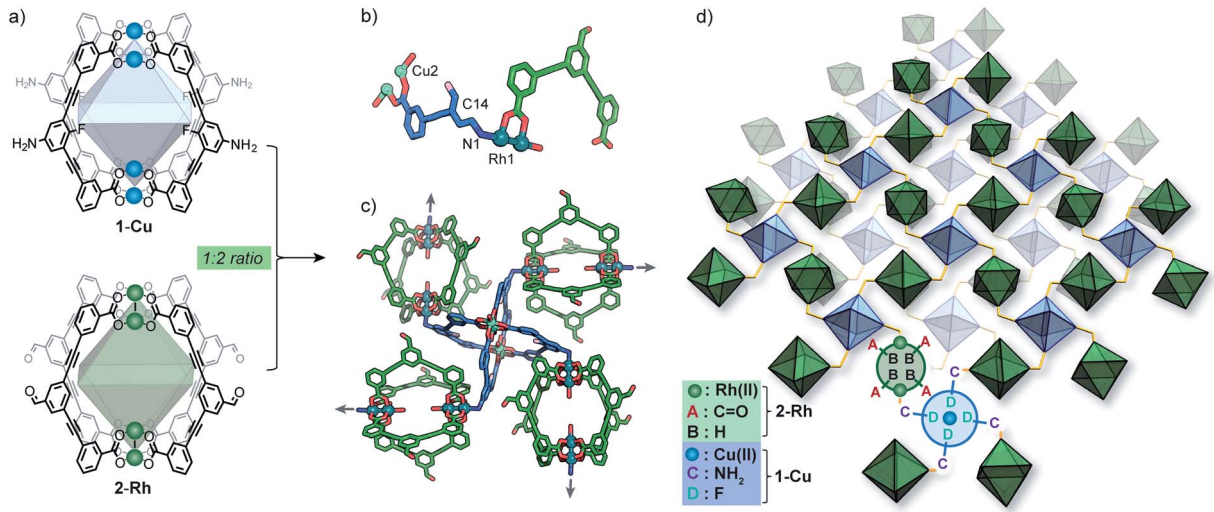


Fig. 2 (a) The molecular structure of **1-Cu** and **2-Rh** and their pairwise linking into a 2-D multivariate MOF $\{[\mathbf{1\text{-}Cu}]\cdot[\mathbf{2\text{-}Rh}]_2\}_n$ (**3**); (b) the asymmetric unit of **3**; (c) a view of **1-Cu** and **2-Rh** as four and two connecting nodes, respectively; (d) a perspective view of the 2-D structure of **3**, where the two MOCs are represented as polyhedra and their ordered functionalities (Rh(II) and Cu(II), A–D) are annotated.

donor from a separate molecule of **1-Cu** ($D_{N1-Rh1}$: 2.23 Å; C14–N1–Rh1: 109.0° – Fig. 2a). Their connectivity is both highly directional and rational; **1-Cu** behaves as a four-connecting node through its exterior aniline donors, whilst **2-Rh** behaves as a two-connecting node through the two exterior paddlewheel sites (Fig. 2c). This combination produces a (4,4)-net, where the 2-D layers pack in a staggered ABAB fashion (Fig. 3c). The eclipsed orientation of **2-Rh** along the *c* axis creates channels approximating the dimensions of internal cavity of the MOC (~7 × 8 Å).

The bulk purity of **3** was confirmed by Powder X-ray Diffraction (PXRD). A Rietveld refinement of the data yielded $R_{wp}$ and GoF (goodness of fit) parameters of 3.89 and 1.15 respectively, indicating that the bulk sample is phase pure and in excellent agreement with the SCXRD structure (Fig. 3a and S10†). This is remarkable given the propensity of **1-Cu** and **2-Rh** to crystallize as discrete structures under similar conditions.[27,31] The 1 : 2 stoichiometry of **1-Cu** and **2-Rh** as observed by SEM/EDX analysis could also be validated by $^1$H NMR spectroscopy. A sample of **3** was dissolved in DMF-$d_7$ by heating which produced a soluble mixture of the pure discrete MOCs in a 1 : 2 ratio, respectively (Fig. S5†). Allowing the solution to stand at 25 °C for 5 days resulted in the re-crystallization of **3** (Fig. 3b and S13†).

Whilst multiple MOC entities are often isolated within MOFs through *in situ* assembly,[32,33] this is the first example where two preformed MOCs have been linked into a multivariate MOF material. Here, the aniline-metal interaction has been precisely tuned to facilitate the pairwise linking of two soluble MOCs upon crystallisation.‡ In doing so, the location and coordination environment of the Cu(II) and Rh(II) metal ions is both predictable and extremely well-defined. In addition, the checkerboard arrangement of **1-Cu** and **2-Rh** results in the ordering of two alternating pore environments, and therefore, multiple ligand-based functionalities (A–D, Fig. 2d).

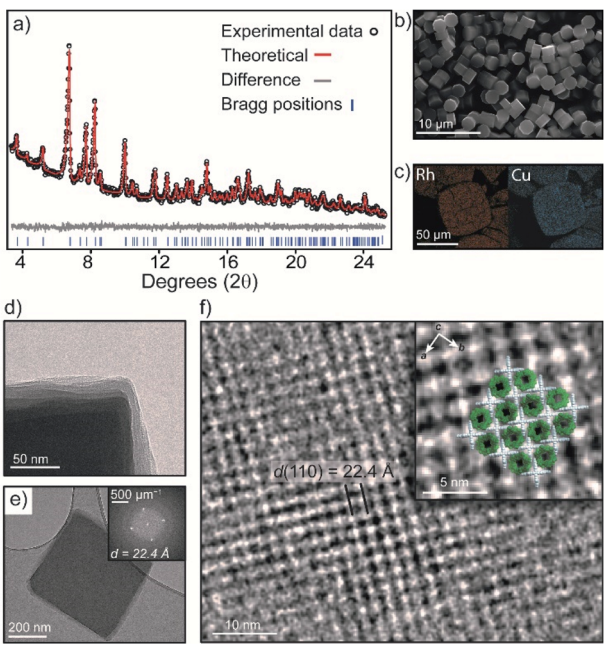


Fig. 3 (a) Rietveld refinement of the PXRD data of **3**; (b) SEM image of **3** obtained from a DMF recrystallization; (c) EDX elemental mapping of Cu and Rh within crystals of **3**; TEM images of **3** (d) the edge of a crystal, showing misalignment of layers; (e) the FFT pattern of a selected crystal; (f) an enlarged image of the same crystal showing the superimposition of the crystal structure of **3** along the *c* axis.

### Activation and porosity of 3

Activation of **3** was carried out by super-critical $CO_2$ exchange of an acetone-solvated sample. Whilst PXRD revealed a reduction in long-range order (Fig. S13†), transmission electron microscopy (TEM) revealed that the MOC ordering within the layers of **3** is largely maintained. An image focused at the edge of a ~400 nm sized crystal clearly shows an irregular alignment of the layers in the activated sample (Fig. 3d). Nevertheless, the Fast Fourier Transform (FFT) pattern in Fig. 3e displays prominent peaks that correspond to a *d* spacing of 22.4 Å. This *d* spacing is in good agreement with the *hkl* 110 plane of **3** (*hkl* 110 = 22.9 Å) which represents the distance between **1-Cu** along the crystallographic *c* axis. In Fig. 3f, the bright regions in the TEM image represent the interconnected **1-Cu** and **2-Rh** MOCs, where **1-Cu** is oriented vertically to the direction of the electron beam. The dark areas correspond to the pores of **2-Rh**, which is oriented perpendicular to the electron beam.

The crystal packing and pore-structure of **3** is clearly dictated by the coordinative linking of **1-Cu** and **2-Rh**. This is in stark contrast to most molecular cage solids, where weak non-covalent interactions are responsible for their solid-state ordering and resulting pore-structure.[34,35] As such, we sought to evaluate the porosity of **3** by $N_2$ and $CO_2$ adsorption measurements at 77 K and 195 K, respectively. The $N_2$ isotherm of **3** displays a typical type-I adsorption profile with a Brunauer–Emmett–Teller surface area ($SA_{BET}$) of 422 $m^2\ g^{-1}$ (Langmuir = 722 $m^2\ g^{-1}$). The pore-size distribution (PSD) derived from the low-pressure region shows a maximum at 8.0 Å (Fig. S18†) which agrees well with the expected dimensions of the internal cavity of **2-Rh**. In contrast, the two discrete MOC solids are non-porous to $N_2$ at 77 K (Fig. S18†), presumably because of the random structural aggregation that accompanies their activation (both solids are amorphous – Fig. S10† and ref. 28). The $CO_2$ isotherms measured 195 K revealed that **1-Cu**, **2-Rh**, and **3** display type I profiles (Fig. S19†). A marked increase in surface area is evident for **3** when comparing to the discrete MOCs; $SA_{BET}$ of **3** = 359 $m^2\ g^{-1}$ (*ca.* 95 and 282 $m^2\ g^{-1}$ for **1-Cu** and **2-Rh**, respectively – Table S1†).

### Stoichiometric control over MOC connectivity and network structure

Given the molecular nature of **1-Cu** and **2-Rh**, we sought to examine whether their connectivity can be dictated by their relative stoichiometry in solution. Owing to their directional linking, we predicted that a change in MOC stoichiometry should result in a change in network structure. Indeed, whilst a 1 : 2 stoichiometry of **1-Cu** and **2-Rh** gave crystals of the 2D MOF **3**, a completely different mixed-cage solid (denoted here as **4**) was obtained from the crystallisation of a 1 : 1 MOC mixture.

Synchrotron SCXRD revealed that **4** crystallizes in the triclinic space group $P\bar{1}$, with a half of each $M_4L_4$ structure in the asymmetric unit. Again, both exterior axial sites of **2-Rh** are coordinated by an aniline donor from a separate molecule of **1-Cu** ($D_{N-Rh}$: 2.22 Å; C–N–Rh: 113.2° – Fig. 4b). Due to the change in stoichiometry, only two of the four aniline donors of **1-Cu** participate in coordination, and the remaining two donors hydrogen bond with co-crystallized DMA solvent; $D_{NH\cdots O} = 2.02$ Å and 2.46 Å, 151.1° and 166.2°, respectively. Thus, both MOCs act as linear two-connecting nodes to give rise to a 1-D coordination polymer with a formula of $\{[\mathbf{1\text{-}Cu}]\cdot[\mathbf{2\text{-}Rh}]\}_n$ (Fig. 4a).

### Elucidating the preference for Rh-aniline coordination by DFT calculations

To rationalize the observed preference for aniline-Rh(II) coordination, we carried out DFT calculations on representative paddlewheel complexes (full details in ESI†). The calculated energy for the ligand exchange reaction shown in Fig. 5a amounts to $\Delta E = -7.6$ kcal mol$^{-1}$ which supports a thermodynamic argument in favour of preferential coordination of aniline to the Rh(II) paddlewheel complex (as compared to the Cu(II) counterpart). For the optimized complexes, the Cu–N bond is ~0.7 Å shorter compared to the Rh–N bond, presumably due to the smaller ionic radius of Cu(II) and the *trans* effect of the Rh(II) complex.[36] This agrees well with the crystallographic results where the Rh–N aniline bond of the linked MOCs is longer by ~0.4 Å compared to Cu–N.[27] Furthermore, the optimized geometry of $[Cu_2(PhCOO)_4(PhNH_2)_2]$ exhibits Cu–O–O–Cu dihedral angles between 14.7° and 15.9° while the corresponding the Rh–O–O–Rh dihedral angles are below 1.3° (Fig. 5b and S32†). The shorter Cu–N bond length and distortion of $[Cu_2(PhCOO)_4(PhNH_2)_2]$ compared to the Rh analogue therefore suggests that the observed preference is associated with a reduced steric hindrance for Rh-aniline coordination. It is noteworthy that $Rh_{24}L_{24}$ MOCs have recently been used to separate regioisomers of methyl pyridine based on their steric hindrance.[37]

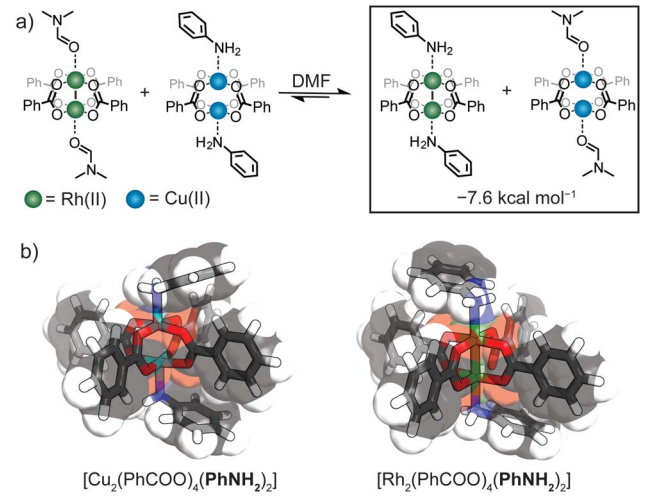


Fig. 5 (a) The ligand exchange reaction between Cu(II) and Rh(II) paddle-wheel complexes as investigated by DFT calculations; (b) a comparison of the optimized structures of $[Cu_2(PhCOO)_4(PhNH_2)_2]$ and $[Rh_2(PhCOO)_4(PhNH_2)_2]$.

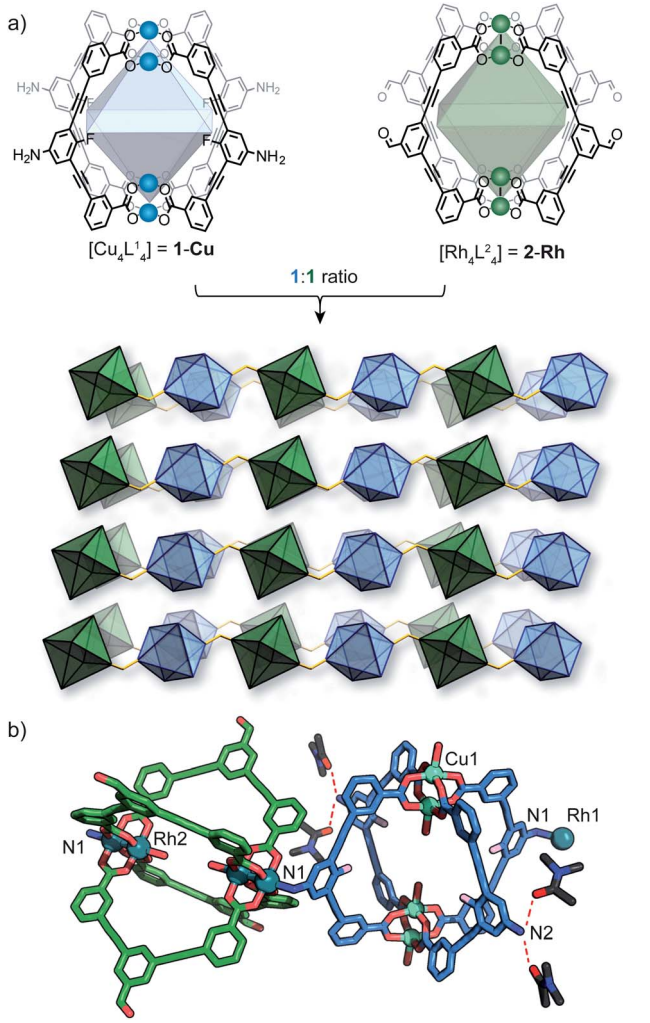


Fig. 4 (a) assembly of $\{[\mathbf{1\text{-}Cu}]\cdot[\mathbf{2\text{-}Rh}]\}_n$ (**4**) from a 1 : 1 mixture of **1-Cu** (left) and **2-Rh** (right) showing a perspective view of the crystal packing (MOCs represented as polyhedra); (b) a view of the coordination of **1-Cu** to **2-Rh**. The bulk characterisation of **4** is described in the ESI.†

## Conclusions

In summary, we have reported the pairwise linking of MOCs as an approach to precisely control the coordination environment and distribution of multiple metal sites and ligands within crystalline porous materials. In doing so, we reported the synthesis and structure of two mixed-cage crystalline solids which can be selectively obtained from the same $Cu_4L_4$ and $Rh_4L_4$ MOC mixture through stoichiometric control. In the case of the 2-D MOF (**3**), the benefit of linking **1-Cu** and **2-Rh** into a mixed-cage network extends also to an improved porosity compared to the discrete cage counterparts. It is worth noting that the selective coordination of **1-Cu** to **2-Rh** also addresses the major challenge of synthesizing coordination polymers from kinetically inert Rh(II) metal ions.[38] Assuming that the

interaction energy and coordination preference are optimised, we expect that this method will extend to a broad range of paddlewheel MOCs[22,39,40] and enable access to a wide range of multi-functional MOFs with control over the connectivity and dimesionality.[41] Indeed, efforts in this direction are currently underway in our laboratory.

## Data availability

We have no extra experimental or computational data associated with this article to deposite.

## Author contributions

WMB: conceptualisation, synthesis, analysis, characterisation (SCXRD, PXRD, TGA, IR, adsorption analysis), writing and editing. AM-H: ligand synthesis and analysis. MR: DFT calculations. ADS: TEM measurements. OL-P: SEM measurements. All authors provided comments and approved the final version of the manuscript.

## Conflicts of interest

There are no conflicts to declare.

## Acknowledgements

W. M. B gratefully acknowledges the Australian Research Council for financially supporting this project (DE190100327). MR thanks the Deutsche Forschungsge-meinschaft (DFG) for funding through Emmy-Noether grant RO 5688/1-1. Jorge Albalad is thanked for advice and helpful discussions. Aspects of this research were undertaken on the MX1 (ref. 42) and MX2 (ref. 43) beamlines at the Australian Synchrotron, Victoria, Australia. The authors acknowledge the instruments and scientific and technical assistance of Microscopy Australia at Adelaide Microscopy, The University of Adelaide, a facility that is funded by the University, and State and Federal Governments.

## Notes and references

‡ The fluoroaniline backbone of $L^1$ is electronically tuned to reduce the possibility of Cu(II)-aniline coordination; phenylene diamine derived ligands were previously observed to interfere with $Cu_4L_4$ MOC assembly.[28] We also attempted to assemble $Cu_4L_4$ MOCs from a pyridyl-functionalised dicarboxylate ligand (ESI†). However, this type of SBB could not be accessed due to the propensity of pyridine to coordinate to Cu(II) during MOC assembly (Fig. S3†). This further demonstrates the importance of tuning the metal–ligand electronics of the linking donor group.

1 W. Xu, B. Tu, Q. Liu, Y. Shu, C.-C. Liang, C. S. Diercks, O. M. Yaghi, Y.-B. Zhang, H. Deng and Q. Li, *Nat. Rev. Mater.*, 2020, **5**, 764–779.
2 A. Kirchon, L. Feng, H. F. Drake, E. A. Joseph and H.-C. Zhou, *Chem. Soc. Rev.*, 2018, **47**, 8611–8638.
3 Y.-B. Huang, J. Liang, X.-S. Wang and R. Cao, *Chem. Soc. Rev.*, 2017, **46**, 126–157.
4 R.-B. Lin, S. Xiang, W. Zhou and B. Chen, *Chem*, 2020, **6**, 337–363.
5 W. Fan, S. Yuan, W. Wang, L. Feng, X. Liu, X. Zhang, X. Wang, Z. Kang, F. Dai, D. Yuan, D. Sun and H.-C. Zhou, *J. Am. Chem. Soc.*, 2020, **142**, 8728–8737.
6 H. Furukawa, K. E. Cordova, M. O'Keeffe and O. M. Yaghi, *Science*, 2013, **341**, 1230444.
7 A. Corma, H. García and F. X. Llabrés i Xamena, *Chem. Rev.*, 2010, **110**, 4606–4655.
8 J. Lee, O. K. Farha, J. Roberts, K. A. Scheidt, S. T. Nguyen and J. T. Hupp, *Chem. Soc. Rev.*, 2009, **38**, 1450–1459.
9 H. Furukawa, U. Müller and O. M. Yaghi, *Angew. Chem., Int. Ed.*, 2015, **54**, 3417–3430.
10 M. Y. Masoomi, A. Morsali, A. Dhakshinamoorthy and H. Garcia, *Angew. Chem., Int. Ed.*, 2019, **58**, 15188–15205.
11 R.-B. Lin, S. Xiang, B. Li, Y. Cui, G. Qian, W. Zhou and B. Chen, *Coord. Chem. Rev.*, 2019, **384**, 21–36.
12 H. Deng, C. J. Doonan, H. Furukawa, R. B. Ferreira, J. Towne, C. B. Knobler, B. Wang and O. M. Yaghi, *Science*, 2010, **327**, 846–850.
13 A. K. Cheetham, G. Kieslich and H. H.-M. Yeung, *Acc. Chem. Res.*, 2018, **51**, 659–667.
14 G. M. Whitesides and B. Grzybowski, *Science*, 2002, **295**, 2418–2421.
15 M. D. Ward and P. R. Raithby, *Chem. Soc. Rev.*, 2013, **42**, 1619–1636.
16 Y.-P. He, G.-H. Chen, D.-J. Li, Q.-H. Li, L. Zhang and J. Zhang, *Angew. Chem., Int. Ed.*, 2021, **60**, 2920–2923.
17 J. T. A. Jones, T. Hasell, X. Wu, J. Bacsa, K. E. Jelfs, M. Schmidtmann, S. Y. Chong, D. J. Adams, A. Trewin, F. Schiffman, F. Cora, B. Slater, A. Steiner, G. M. Day and A. I. Cooper, *Nature*, 2011, **474**, 367–371.
18 A. J. Gosselin, A. M. Antonio, K. J. Korman, M. M. Deegan, G. P. A. Yap and E. D. Bloch, *J. Am. Chem. Soc.*, 2021, **143**, 14956–14961.
19 G. R. Desiraju, *Nat. Mater.*, 2002, **1**, 77–79.
20 A. Pulido, L. Chen, T. Kaczorowski, D. Holden, M. A. Little, S. Y. Chong, B. J. Slater, D. P. McMahon, B. Bonillo, C. J. Stackhouse, A. Stephenson, C. M. Kane, R. Clowes, T. Hasell, A. I. Cooper and G. M. Day, *Nature*, 2017, **543**, 657–664.
21 D. J. Tranchemontagne, Z. Ni, M. O'Keeffe and O. M. Yaghi, *Angew. Chem., Int. Ed.*, 2008, **47**, 5136–5147.
22 S. Lee, H. Jeong, D. Nam, M. S. Lah and W. Choe, *Chem. Soc. Rev.*, 2021, **50**, 528–555.
23 J. R. Li, D. J. Timmons and H. C. Zhou, *J. Am. Chem. Soc.*, 2009, **131**, 6368–6369.
24 T. Grancha, A. Carné-Sánchez, F. Zarekarizi, L. Hernández-López, J. Albalad, A. Khobotov, V. Guillerm, A. Morsali, J. Juanhuix, F. Gándara, I. Imaz and D. Maspoch, *Angew. Chem., Int. Ed.*, 2021, **60**, 5729–5733.
25 H.-N. Wang, X. Meng, G.-S. Yang, X.-L. Wang, K.-Z. Shao, Z.-M. Su and C.-G. Wang, *Chem. Commun.*, 2011, **47**, 7128–7130.
26 H.-N. Wang, F.-H. Liu, X.-L. Wang, K.-Z. Shao and Z.-M. Su, *J. Mater. Chem. A*, 2013, **1**, 13060–13063.
27 M. L. Schneider, A. W. Markwell-Heys, O. M. Linder-Patton and W. M. Bloch, *Front. Chem.*, 2021, **9**, 382.

28 M. L. Schneider, O. M. Linder-Patton and W. M. Bloch, *Chem. Commun.*, 2020, **56**, 12969–12972.
29 G. A. Taggart, A. M. Antonio, G. R. Lorzing, G. P. A. Yap and E. D. Bloch, *ACS Appl. Mater. Interfaces*, 2020, **12**, 24913–24919.
30 H. Furukawa, J. Kim, N. W. Ockwig, M. O'Keeffe and O. M. Yaghi, *J. Am. Chem. Soc.*, 2008, **130**, 11650–11661.
31 W. M. Bloch, R. Babarao and M. L. Schneider, *Chem. Sci.*, 2020, **11**, 3664–3671.
32 J. J. Perry IV, J. A. Perman and M. J. Zaworotko, *Chem. Soc. Rev.*, 2009, **38**, 1400–1417.
33 V. Guillerm, D. Kim, J. F. Eubank, R. Luebke, X. Liu, K. Adil, M. S. Lah and M. Eddaoudi, *Chem. Soc. Rev.*, 2014, **43**, 6141–6172.
34 T. Tozawa, J. T. A. Jones, S. I. Swamy, S. Jiang, D. J. Adams, S. Shakespeare, R. Clowes, D. Bradshaw, T. Hasell, S. Y. Chong, C. Tang, S. Thompson, J. Parker, A. Trewin, J. Bacsa, A. M. Z. Slawin, A. Steiner and A. I. Cooper, *Nat. Mater.*, 2009, **8**, 973–978.
35 E. J. Gosselin, C. A. Rowland and E. D. Bloch, *Chem. Rev.*, 2020, **120**, 8987–9014.
36 Y. B. Koh and G. G. Christoph, *Inorg. Chem.*, 1978, **17**, 2590–2596.
37 L. Hernández-López, J. Martínez-Esaín, A. Carné-Sánchez, T. Grancha, J. Faraudo and D. Maspoch, *Angew. Chem., Int. Ed.*, 2021, **60**, 11406–11413.
38 W.-Y. Gao, A. Sur, C.-H. Wang, G. R. Lorzing, A. M. Antonio, G. A. Taggart, A. A. Ezazi, N. Bhuvanesh, E. D. Bloch and D. C. Powers, *Angew. Chem., Int. Ed.*, 2020, **59**, 10878–10883.
39 S. Furukawa, N. Horike, M. Kondo, Y. Hijikata, A. Carné-Sánchez, P. Larpent, N. Louvain, S. Diring, H. Sato, R. Matsuda, R. Kawano and S. Kitagawa, *Inorg. Chem.*, 2016, **55**, 10843–10846.
40 E.-S. M. El-Sayed and D. Yuan, *Chem. Lett.*, 2019, **49**, 28–53.
41 V. Guillerm and M. Eddaoudi, *Acc. Chem. Res.*, 2021, **54**, 3298–3312.
42 N. P. Cowieson, D. Aragao, M. Clift, D. J. Ericsson, C. Gee, S. J. Harrop, N. Mudie, S. Panjikar, J. R. Price, A. Riboldi-Tunnicliffe, R. Williamson and T. Caradoc-Davies, *J. Synchrotron Radiat.*, 2015, **22**, 187–190.
43 D. Aragão, J. Aishima, H. Cherukuvada, R. Clarken, M. Clift, N. P. Cowieson, D. J. Ericsson, C. L. Gee, S. Macedo, N. Mudie, S. Panjikar, J. R. Price, A. Riboldi-Tunnicliffe, R. Rostan, R. Williamson and T. T. Caradoc-Davies, *J. Synchrotron Radiat.*, 2018, **25**, 885–891.